Chapter-4

K & Ga Doped $BaZrO_3$ as Oxide-ion Conductor

4.1 Introduction

$BaZrO_3$ is a well-known ceramic in cubic perovskite structure and recently gained considerable attention due to its application as a proton conductor electrolyte in ceramic fuel cells and hydrogen separation membranes with doping of Y on Zr sites.[1-2] The higher protonic conductivity of $BaZr_{1-x}Y_xO_{3-x/2}$ decreases severely at elevated temperature (T > 600^{o}C) due to its inability to hold moisture/water or adsorbed water from moist air or fuel to retain its protonic conductivity. Due to this, $BaZr_{1-x}Y_xO_{3-x/2}$ has not been suitable as an electrolyte for fuel cells. High ionic conductivity at elevated temperature (T >500^{o}C) is a critical requirement for its application as an electrolyte for ceramic fuel cells. Due to the high resultant strain on the structure coupled with relatively higher size Y^{3+} compared to Zr^{4+}, the doping level of Y on the Zr site is kept low, resulting in a lower concentration of oxide-ion vacancies; hence lower the conductivities by oxide-ion vacancies type point defects.[3-4]

In most of the perovskite and fluorite-based materials studied, Oxide-ion conductivity gets better at higher temperatures in the mobile oxide-ion vacancy conduction model.[5-10] Therefore, we have envisaged the simultaneous doping of smaller Ga on the Zr site and K on the Ba site to create a higher concentration of oxide-ion vacancies to realize superior conductivities. Due to its robust structure in the cubic perovskite phase, vacancy migration probability increases. This chapter presents the synthesis, characterization, and ionic conductivity studies of K and Ga doped $BaZrO_3$ samples. The higher degree of simultaneous substitution of K and Ga created a higher degree of oxygen vacancies type defects, resulting in higher oxide-ion conductivity.

4.2 Material synthesis and characterization

$Ba_{1-x}K_xZr_{1-y}Ga_yO_{3-\delta}$ samples were synthesized by solid-state ceramic route by mixing stoichiometric amounts of $BaCO_3$, K_2CO_3, ZrO_2 and Ga_2O_3, subsequently heating them for 15 hours at 1150°C. For obtaining the single-phase material, multiple heating cycles were carried out. Samples were heated thrice at 1150°C for 15 hours with an intermediate grounding of the sample. For conductivity measurement, the powder was made into pellets of 10 mm diameter and ~0.2-0.25cm thickness by pressing it to 6-7 ton weight on a hydraulic press. These pellets were fired at 1200°C for 10 hours for densification. The pellet density was measured using the Archimedes method, and it was found to be ~97% of the theoretical density of the material.

The phase formation study was carried out through Rigaku Miniflex desktop X-ray Diffractometer (XRD) with Cu-Kα radiation (λ = 1.54 Å) in the range 2θ ~ 10 - 90° with a step size of 0.02°. The structures were refined by the Rietveld refinement method using FULLPROF suite software package[11] and cubic perovskite $BaZrO_3$ (space group: Pm3m) as model structure. The microstructures of the sintered samples were investigated by using scanning electron microscopy (EVO - Scanning Electron Microscope MA15/18). The average grain size was calculated using the linear intercept method. The composition of the compounds was examined by Energy dispersive X-ray (EDX) spectroscopy with a probe attached to the SEM instrument.

The total conductivity measurements of all the samples were carried out using an impedance analyser, AUTOLAB, the Netherlands, from 1MHz to 1 Hz in the temperature range 300 °C to 650°C in different atmospheres. The sintered pellets were coated with silver paste and cured at 500 °C for 30 min. Platinum wire was used as a contact for current

collector. The total conductivity of the samples is determined from the intercepts of the semicircle on the real axis by using the following relationship:

$$\sigma = l/RA \ Scm^{-1} \qquad \text{eq(4.1).}$$

where l/A is the geometrical factor, l is the thickness; A is the area of the sample, and R is the total resistance which is indicated by the intercept of the semicircle on the real axis. All measurements were taken during the cooling cycle from 650°C to 100°C.

4.3 Results and discussion

4.3.1 XRD Study

Up to 25% of K at Ba site and 25% Ga at Zr site simultaneously substituted $BaZrO_3$ lattice. The synthesized K and Ga substituted $BaZrO_3$ powders were off white in colour, while the undoped $BaZrO_3$ was a pure white colour sample. (Figure 4.1)

Figure 4.1 Photograph of synthesized powder (off-white colour) & $BaZrO_3$

The crystal structure and phase purity of the material were studied by powder XRD. Powder XRD pattern of $Ba_{0.9}K_{0.1}Zr_{0.9}Ga_{0.1}O_{2.9}$, $Ba_{0.85}K_{0.15}Zr_{0.85}Ga_{0.15}O_{2.85}$,

$Ba_{0.8}K_{0.2}Zr_{0.8}Ga_{0.2}O_{2.8}$ and $Ba_{0.75}K_{0.25}Zr_{0.75}Ga_{0.25}O_{2.75}$ are shown Figure 4.2(b-d) respectively. All the peaks were identified as $BaZrO_3$ structures (JCPDS No: 98-007-6499). XRD pattern of most samples (except $Ba_{0.8}K_{0.2}Zr_{0.8}Ga_{0.2}O_{2.8}$) contains the weak reflection for $BaCO_3$ diffraction peaks (JCPDS No: 98-000-5968). Barium is known for its very high affinity for CO_2 due to its high basicity.

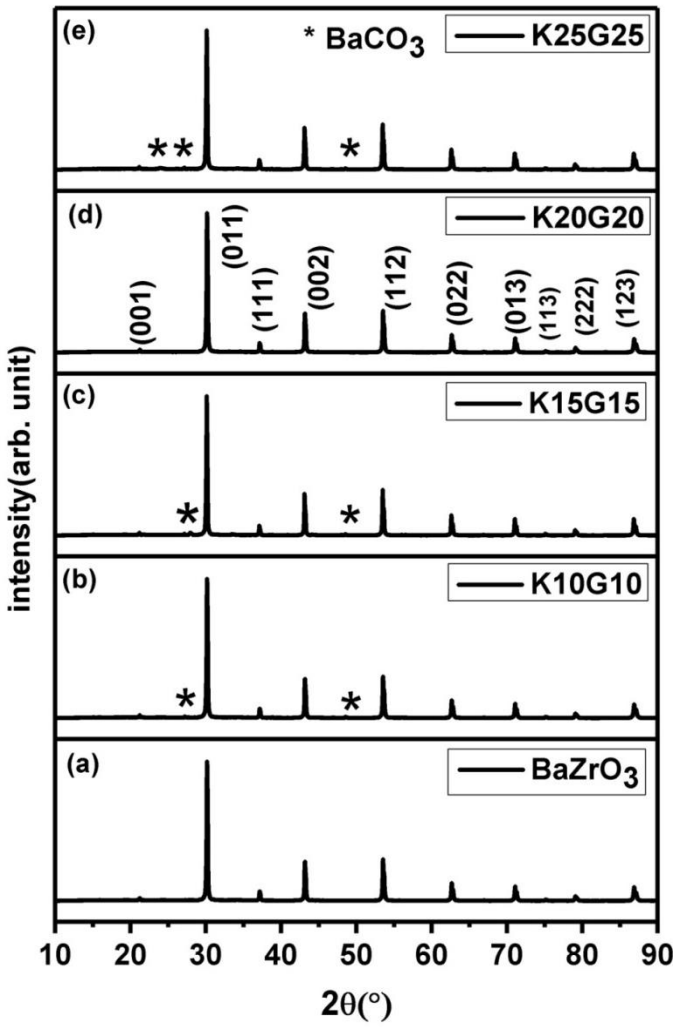

Figure 4.2 Powder XRD pattern (a) $BaZrO_3$ (b)$Ba_{0.9}K_{0.1}Zr_{0.9}Ga_{0.1}O_{2.9}$ (K10G10) (c) $Ba_{0.85}K_{0.15}Zr_{0.85}Ga_{0.15}O_{2.85}$ (K15G15) (d) $Ba_{0.8}K_{0.2}Zr_{0.8}Ga_{0.2}O_{2.8}$ (K20G20) (e) $Ba_{0.75}K_{0.25}Zr_{0.75}Ga_{0.25}O_{2.75}$ (K25G25)

Thus, the minute level impurities peaks may arrive due to the presence of some unreacted $BaCO_3$ precursor utilized for synthesis or formation $BaCO_3$ on the surface due to

CO_2 absorption. All the samples were kept long before we did a primary XRD study of the materials for comparison. No other reflections can be seen in the powder XRD pattern for any of the Ga_2O_3 and K_2CO_3 phases in $Ba_{1-x}K_xZr_{1-x}Ga_xO_{3-x}$ samples. There is a systematic increase in the lattice parameter of $Ba_{1-x}K_xZr_{1-x}Ga_xO_{3-x}$ with increasing K and Ga content, except for the x = 0.2 sample that shows the highest conductivity as 2θ shifted to a lower value with an increase in doping concentration (Figure4.3).

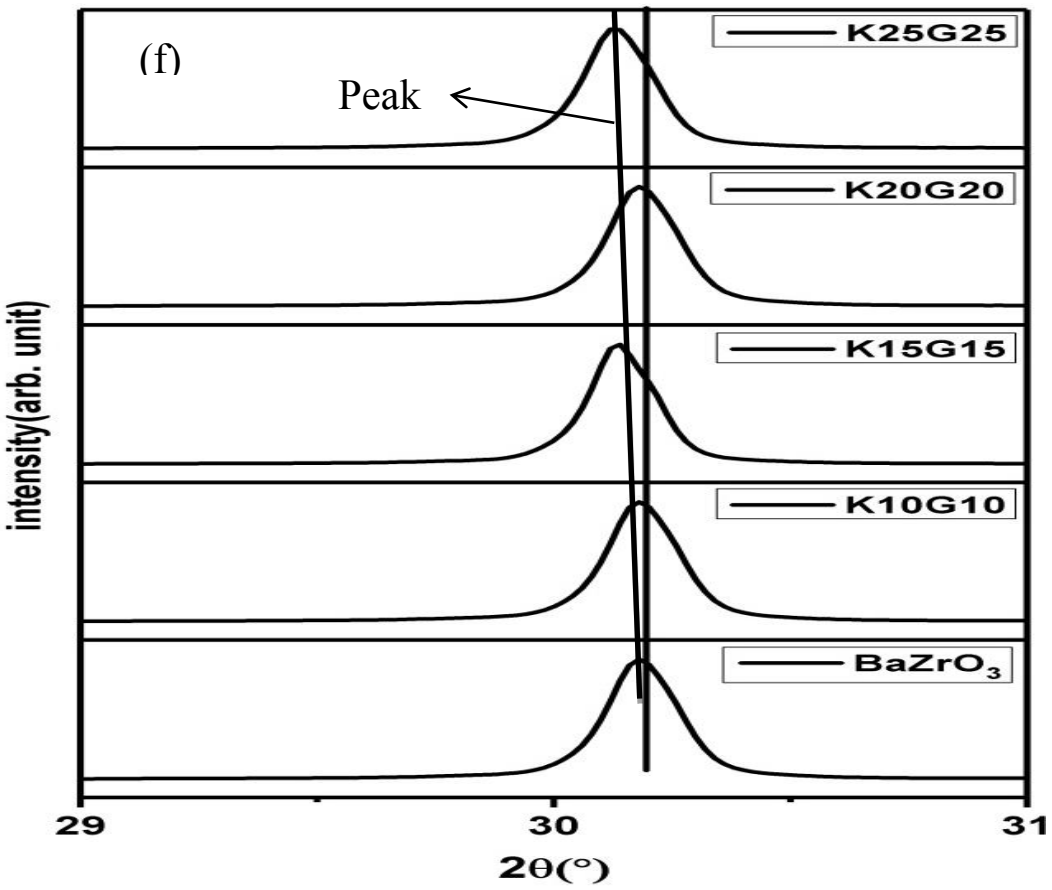

Figure 4.3 shows the systematic peak shift of (011) plane of $Ba_{1-x}K_xZr_{1-x}Ga_xO_{3-x}$ (x = 0. 0.1, 0.15, 0.2 and 0.25) samples with doping.

Crystal structures of K and Ga substituted $BaZrO_3$ were refined using the Rietveld method. For this purpose, XRD of preheated samples was recorded at a slow scan rate 1^o per minute with 0.01^o step size. Figure 4.4 shows the Rietveld refined XRD profile of (a)

$Ba_{0.9}K_{0.1}Zr_{0.9}Ga_{0.1}O_{2.9}$, (b) $Ba_{0.85}K_{0.15}Zr_{0.85}Ga_{0.15}O_{2.85}$ (c) $Ba_{0.8}K_{0.2}Zr_{0.8}Ga_{0.2}O_{2.8}$ (d) $Ba_{0.75}K_{0.25}Zr_{0.75}Ga_{0.25}O_{2.74.}$ The fitted profile matched well with the observed XRD pattern. In preheated $Ba_{0.75}K_{0.25}Zr_{0.75}Ga_{0.25}O_{3-\delta}$ sample shown in Figure 4.4(d), we still got a weak reflection for the $BaCO_3$ phase (JCPDS No:98-007-6499).

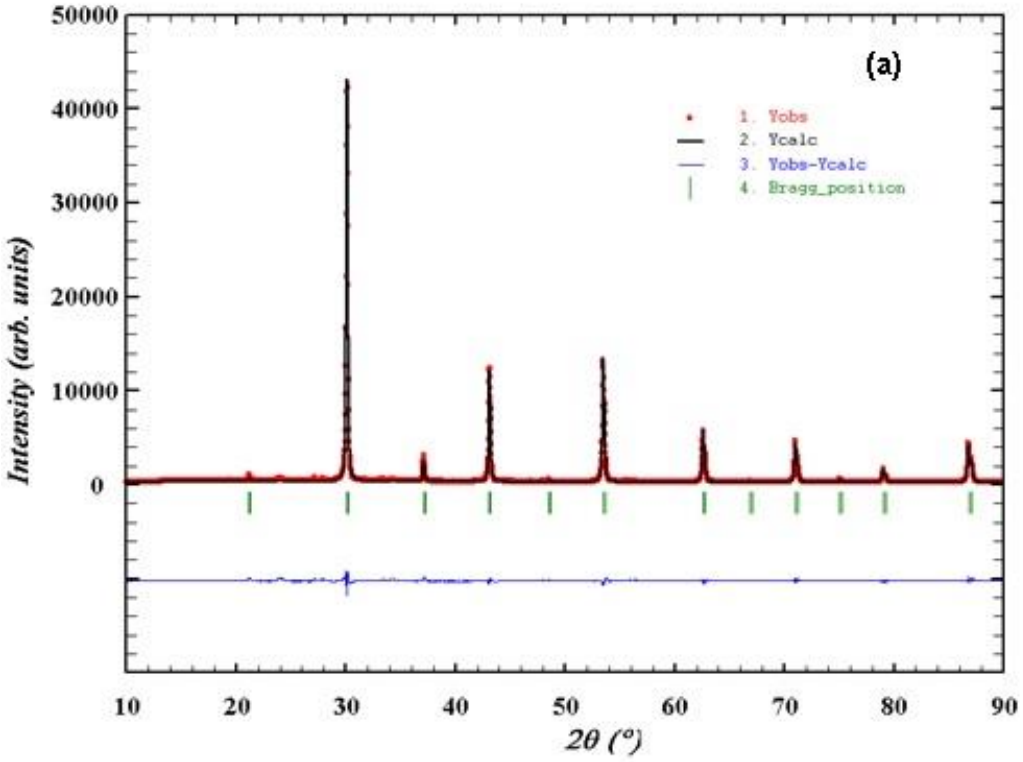

Figure 4.4. (a) Rietveld refined powder XRD profile of $Ba_{0.9}K_{0.1}Zr_{0.9}Ga_{0.1}O_{2.9}$

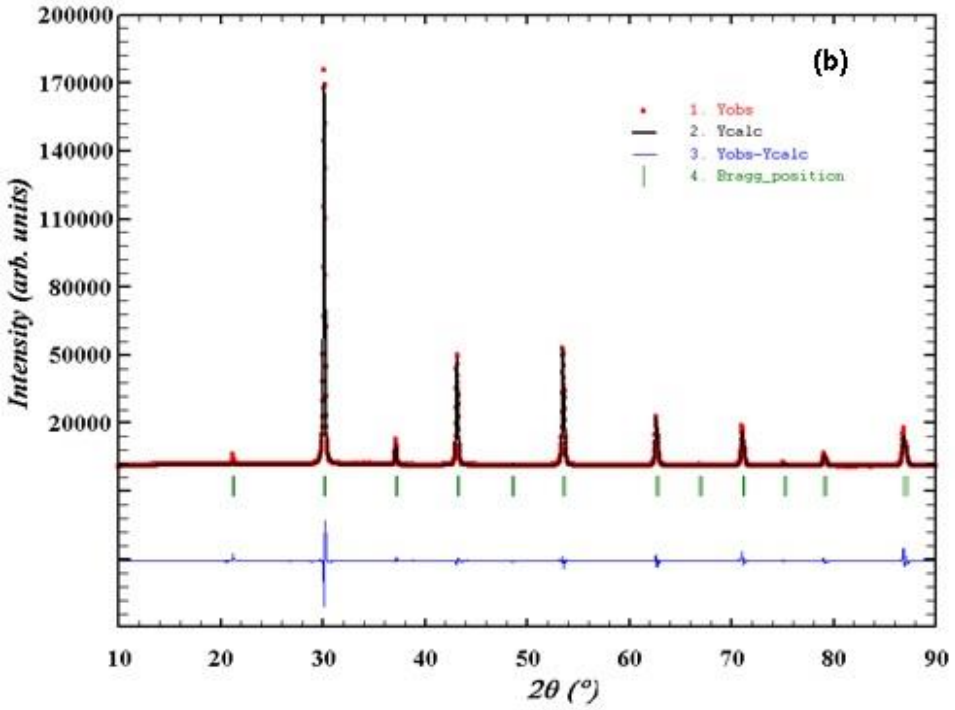

Figure 4.4. (b) Rietveld refined powder XRD profile of $Ba_{0.85}K_{0.15}Zr_{0.85}Ga_{0.15}O_{2.85}$

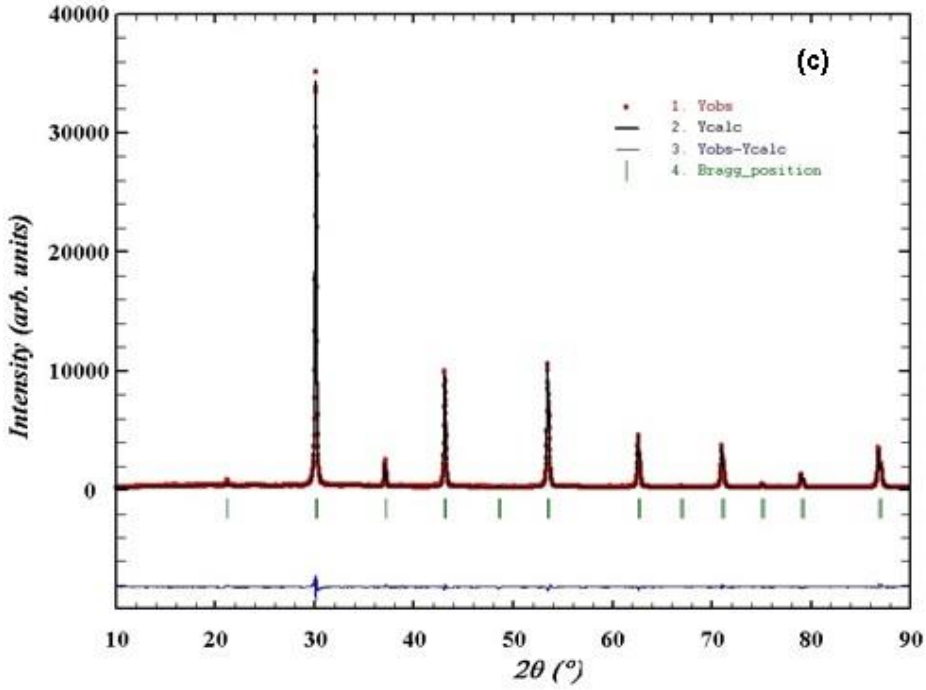

Figure 4.4. (c) Rietveld refined powder XRD profile of $Ba_{0.8}K_{0.2}Zr_{0.8}Ga_{0.2}O_{2.8}$

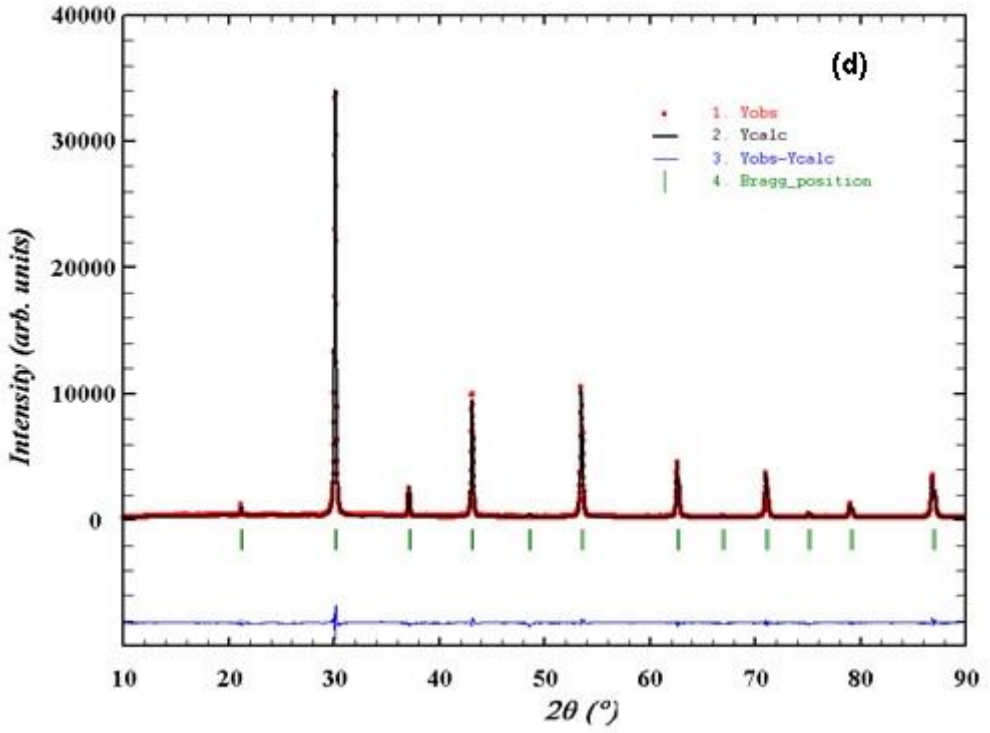

Figure 4.4. (d) Rietveld refined powder XRD profile of $Ba_{0.75}K_{0.25}Zr_{0.75}Ga_{0.25}O_{2.75}$

The structural parameters obtained from reitveld refinement of powder XRD pattern are given in Table 4.1. The lattice parameter of $BaZrO_3$ was found at 4.191Å, and for $Ba_{0.75}K_{0.25}Zr_{0.75}Ga_{0.25}O_{2.75}$, it was found to be 4.194Å. The lattice parameter of $Ba_{0.8}K_{0.2}Zr_{0.8}Ga_{0.2}O_{2.8}$ was also found 4.194 Å (higher than the lattice parameter of undoped $BaZrO_3$).

Table 4.1: Structural parameter of K and Ga doped $BaZrO_3$

Compound	Lattice parameter(Å) (a=b=c)	χ^2	R_f	R_{Bragg}
$BaZrO_3$	*4.1910(1)*	1.03	2.12	1.04
$Ba_{0.9}K_{0.1}Zr_{0.9}Ga_{0.1}O_{2.9}$	4.1937(2)	3.05	4.14	2.87
$Ba_{0.85}K_{0.15}Zr_{0.85}Ga_{0.15}O_{2.85}$	4.1940(1)	1.46	1.17	1.30
$Ba_{0.8}K_{0.2}Zr_{0.8}Ga_{0.2}O_{2.8}$	4.1914(2)	0.89	1.08	1.26
$Ba_{0.75}K_{0.25}Zr_{0.75}Ga_{0.25}O_{2.75}$	4.1940(2)	4.10	4.11	1.98

The substitution of K^+ and Ga^{3+} on Ba & Zr sites, respectively, in $BaZrO_3$ lattice, show little increase in the lattice parameter with an increase in doping except for $Ba_{0.8}K_{0.2}Zr_{0.8}Ga_{0.2}O_{2.8}$ sample. Point to be noted that K^+ ion is slightly bigger than Ba^{2+} ion in 12 coordination and Ga^{3+} smaller than Zr^{4+} ion in six coordination.[12] Thus, due to the rigid nature of the octahedral network in the 3-d structure of the perovskite lattice and compensation due to different size cations (K^+ and Ga^{3+} ions substitution in the $BaZrO_3$ lattice) results in only little change in the lattice parameter of doped $BaZrO_3$ based perovskites.

4.3.2 Thermal Study

As barium is known to have a very high affinity for H_2O and CO_2, TGA/DSC studies were carried out to know the weight loss due to water/moisture absorption and desorption on the materials and the associated phase changes that may occur due to this. As preheated sample of $Ba_{0.8}K_{0.2}Zr_{0.8}Ga_{0.2}O_{2.8}$ was thermal analyzed in thermo gravimetric and differential scanning calorimetry (TGA-DSC) analysis at a constant heating rate of 10^oC/minute in the temperature range of 30^oC – 900^oC & in N_2 atmosphere. Figure 4.5 demonstrates the TGA and DSC curves of the pure $Ba_{0.8}K_{0.2}Zr_{0.8}Ga_{0.2}O_{2.8}$ sample preheated at 200^oC. The first stage of weight loss between 100°C to 200°C is due to the loss of the adsorbed moisture and structural water present in the sample after exposure to the atmosphere. The second stage of weight loss, around 400-600°C, is due to the removal of absorbed or strongly bonded carbonaceous species present in the materials and is attributed to the final phase formation. TGA study confirms the materials relatively low hygroscopic nature (0.8% weight loss up to 400^oC and a total 1.5% weight loss up to 700^oC) and absence of absorbed moisture in the sample above 400^oC. The DSC curve shown in Figure 4.5 does not show any significant feature for any associated phase change that may arrive from oxide-ion vacancy or structure reorientation. Thus the TGA/DSC studies confirm the structural stability of the material in the temperature range of 30^oC-900^oC.

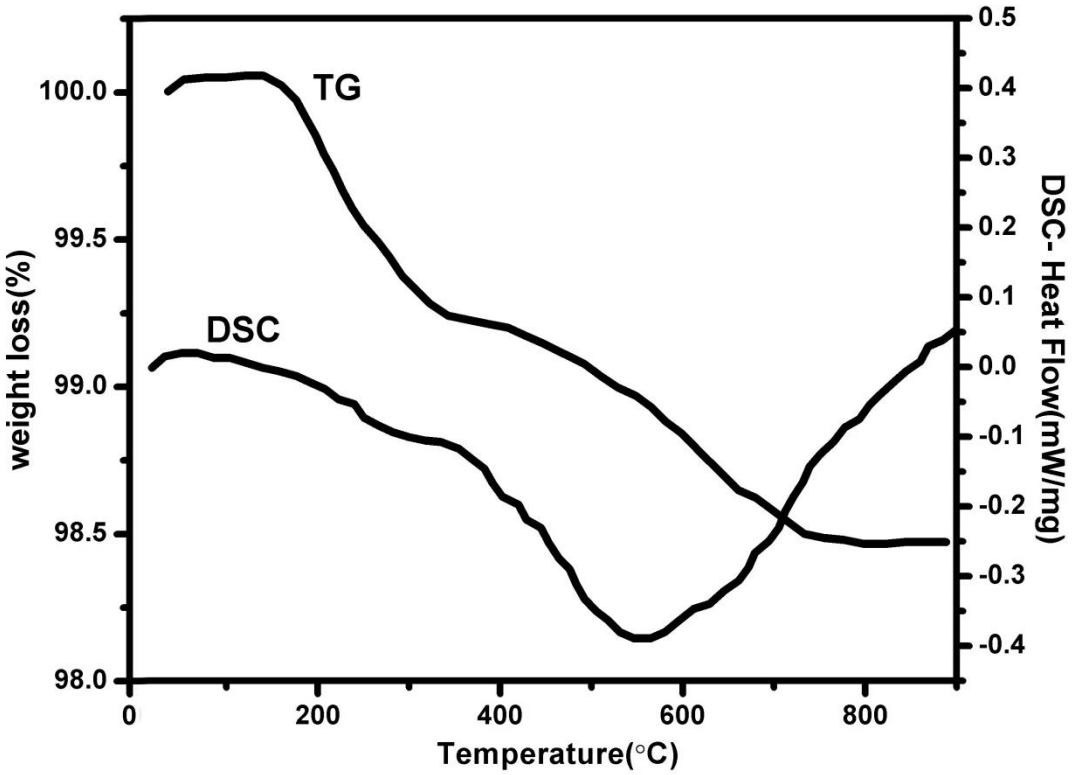

Figure 4.5 Thermogravimetric analysis (TGA) & DSC curve of $Ba_{0.8}K_{0.2}Zr_{0.8}Ga_{0.2}O_{2.8}$

4.3.3 SEM Study

SEM micrographs of $Ba_{0.8}K_{0.2}Zr_{0.8}Ga_{0.2}O_{2.8}$ (powder, front view and cross-section of the pellet utilized for conductivity measurement) are given in Figure 4.6(a-c). The SEM study reveals that the powder sample contains dense grains of 3–8μm in size. No colour contrast was observed in the SEM images suggesting a single phase of the materials forming the grains. Figure 4.6(b and c) also shows the images of the front and cross-section of the pellet. The microstructure of the pellets is showing a good density of the pellet, and the grains are in good contact with each other due to crystal growth during sintering. The EDX study with the probe attached to the SEM instrument (micrograph shown in Figure 4.6(d)) also confirms that the composition of the materials is close to the nominal composition taken for the synthesis of the material.

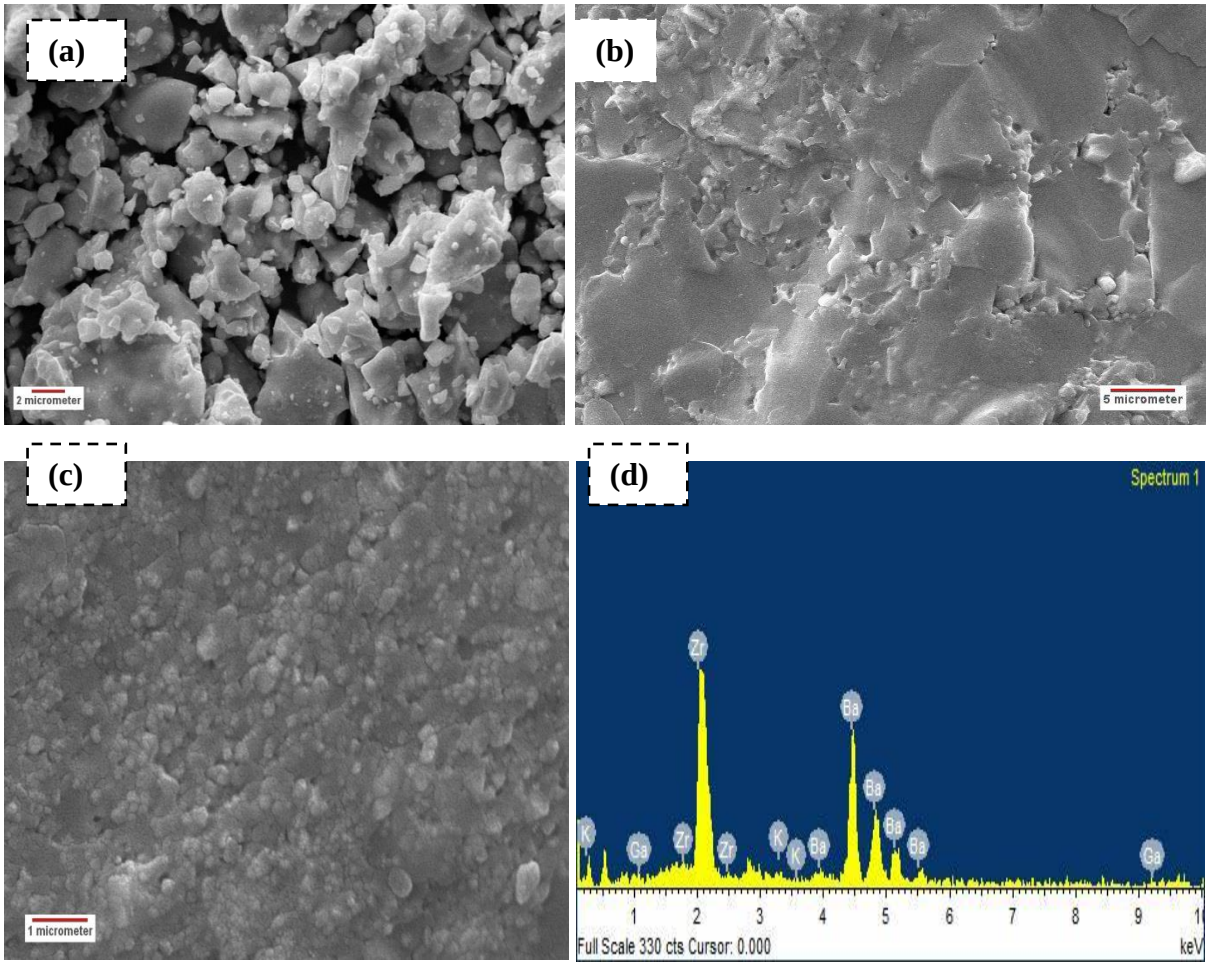

Figure 4.6. SEM image $Ba_{0.8}K_{0.2}Zr_{0.8}Ga_{0.2}O_{2.8}$ (a) Powder (b) Front view of the pellet (c) Cross-section of the pellets and (d) image of EDX spectra

4.3.4 TEM Study

TEM investigation of the powder $Ba_{0.8}K_{0.2}Zr_{0.8}Ga_{0.2}O_{2.8}$ sample reveals the agglomeration of particles (Figure 4.7(a, b). In Figure 4.7(c), the Electron diffraction image shows the diffraction rings of various planes (011) and (111) that are consistent with the XRD indexing of the powder sample (Figure 4.2). HRTEM image in Figure 4.7(d)) shows the lattice fringes of the sample, and the spacing between the adjacent lattice fringes, calculated as 2.96Å, was assigned to the (011) plane of $Ba_{0.8}K_{0.2}Zr_{0.8}Ga_{0.2}O_{2.8}$. With HRTEM, Elemental mapping of the sample $Ba_{0.8}K_{0.2}Zr_{0.8}Ga_{0.2}O_{2.8}$ clearly shows that the sample is composed of Ba, Zr, O, K,

Ga without any impurity elements. The EDS mapping ensures that all the elements are uniformly distributed over the cubic structure of nano powder (Figure 4.7(e)).

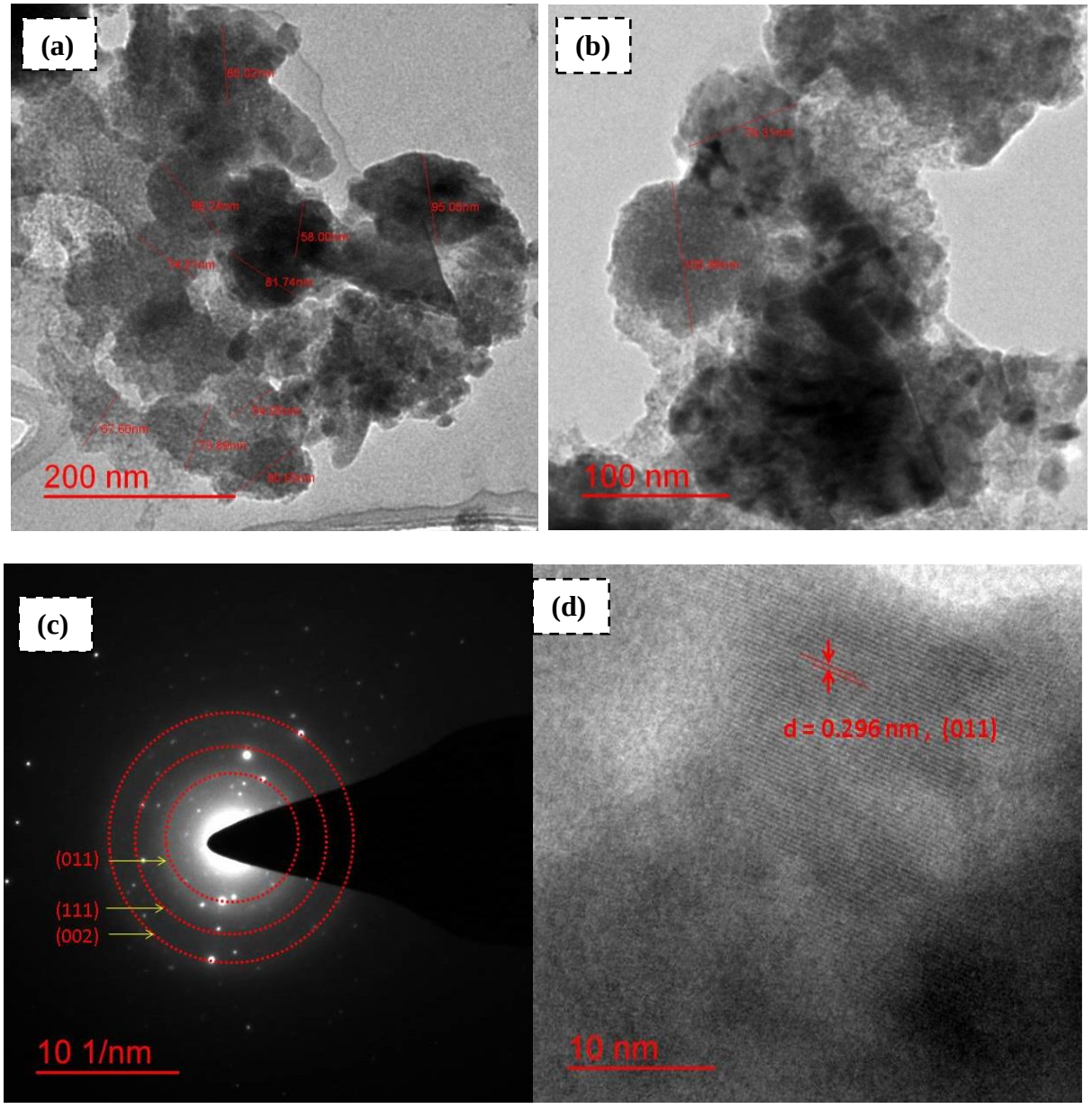

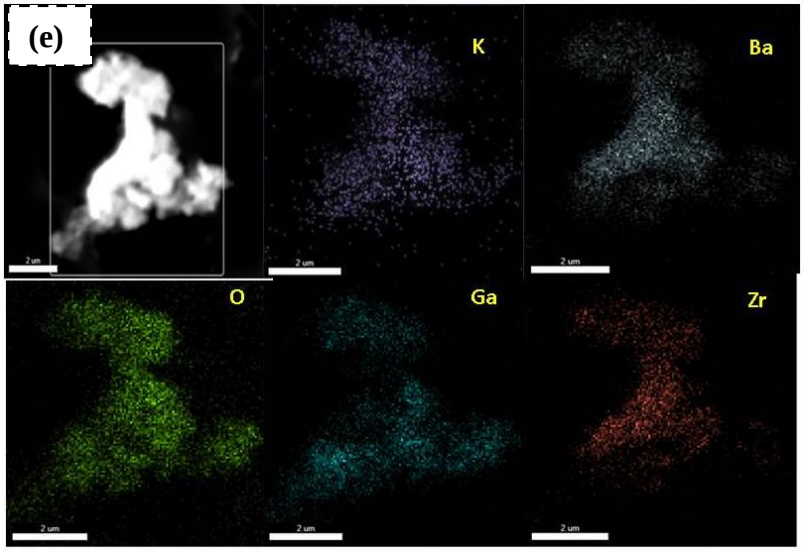

Figure 4.7. (a) & (b) TEM image Powder $Ba_{0.8}K_{0.2}Zr_{0.8}Ga_{0.2}O_{2.8}$ (c) SAED pattern from $Ba_{0.8}K_{0.2}Zr_{0.8}Ga_{0.2}O_{2.8}$ (d) HRTEM of $Ba_{0.8}K_{0.2}Zr_{0.8}Ga_{0.2}O_{2.8}$ Showing (011) planes (e) Elemental mapping of the $Ba_{0.8}K_{0.2}Zr_{0.8}Ga_{0.2}O_{2.8}$.

Thus XRD, SEM, and HRTEM coupled with EDX study confirm that K^+ and Ga^{3+} ion are substituted in $BaZrO_3$ lattice respectively at Ba^{3+} and Zr^{4+} sites. Considering the intrinsic stoichiometric defects, the substitution of K^+ at Ba^{2+} site and substitution of Ga^{3+} and Zr^{4+} will create oxygen vacancy formation and the defect formation equation using Kröger–Vink notation can be represented as:

$$K_{Ba}^{'} + Ga_{Zr}^{'} \leftrightarrow V_o^{\cdot\cdot} \qquad \text{Eq (4.2)}$$

4.3.5 Impedance Study

Oxide-ion conductivity or total ionic conductivity studies of the materials were carried out using an impedance spectrometer at various temperatures in different environments. Figure 4.8 show the oxide-ion conductivity for different composition of K and Ga substituted $BaZrO_3$ i.e. (i) $Ba_{0.9}K_{0.1}Zr_{0.9}Ga_{0.1}O_{2.9}$ (ii) $Ba_{0.85}K_{0.15}Zr_{0.85}Ga_{0.15}O_{2.85}$ (iii) $Ba_{0.8}K_{0.2}Zr_{0.8}Ga_{0.2}O_{2.8}$ (iv) $Ba_{0.75}K_{0.25}Zr_{0.75}Ga_{0.25}O_{2.74.}$ The conductivity was found continuously increase with increasing temperature for all the compositions. The best oxide-ion conductivity of this series was observed for the composition $Ba_{0.8}K_{0.2}Zr_{0.8}Ga_{0.2}O_{2.8,}$ and at

650°C, the measured oxide-ion conductivity was ~10^{-2} S.cm^{-1} for the material. A sudden increase in oxide-ion conductivity was observed over 400°C of all the samples except $Ba_{0.8}K_{0.2}Zr_{0.8}Ga_{0.2}O_{2.8}$. We also calculated the activation energy of conduction using the Arrhenius equation below 400°C and above 400°C. The change in conductivity and activation energy is very similar for the reported perovskite oxide-ion conductors such as $La_{1-x}Sr_xGa_{1-y}Mg_yO_{3-(x+y)/2}$ [13-16] and $Na_{0.5}Bi_{0.5}TiO_3$ [7-8]. We believe in K and Ga doped $BaZrO_3$ based system also the same mechanism of mobile vacancy percolation is occurring. The conductivity presented here for the $Ba_{0.8}K_{0.2}Zr_{0.8}Ga_{0.2}O_{2.8}$ sample is better or equivalent to the conductivity obtained for YSZ (yttria-stabilized zirconia); a well known ceramic oxide-ion electrolyte employed solid oxide fuel cells. Table 4.2 presents the conductivities of different compounds commonly used as oxide-ion electrolytes for SOFCs.

Table 4.2 O^{2-} conductivity (σ) of $Ba_{1-x}K_xZr_{1-y}Ga_yO_{3-\delta}$ at different temperatures

	Conductivity (S.cm^{-1})			
Compound	***650°C***	**600°C**	**550°C**	**500°C**
$Ba_{0.9}K_{0.1}Zr_{0.9}Ga_{0.1}O_{2.9}$	$8.6x10^{-4}$	$4.1x10^{-4}$	$2.8x10^{-4}$	$1.6x10^{-4}$
$Ba_{0.85}K_{0.15}Zr_{0.85}Ga_{0.15}O_{2.85}$	$1.1x10^{-3}$	$4.5x10^{-4}$	$4.4x10^{-4}$	$1.6x10^{-4}$
$Ba_{0.8}K_{0.2}Zr_{0.8}Ga_{0.2}O_{2.8}$	**$2.1x10^{-2}$**	**$8.8x10^{-3}$**	**$3.3x10^{-3}$**	**$1.6x10^{-3}$**
$Ba_{0.75}K_{0.25}Zr_{0.75}Ga_{0.25}O_{2.75}$	$8.9x10^{-3}$	$4.3x10^{-3}$	$2.1x10^{-2}$	$8.9x10^{-4}$
$KTa_{0.4}Ti_{0.3}Ge_{0.3}O_{2.7}$ (Ref. 10)	$4.2x10^{-2}$	$3.1x10^{-2}$	$9.8x10^{-3}$	$8.5x10^{-3}$
$Na_{0.5}Bi_{0.49}Ti_{0.98}Mg_{0.02}O_{2.965}$ (Ref 7)		$4.6x10^{-3}$	$4.4x10^{-3}$	$3.5x10^{-3}$
$Zr_{0.92}Y_{0.08}O_{1.96}$ (Ref. 7)		$4.4x10^{-3}$	$2.3x10^{-3}$	$1x10^{-3}$
$Ce_{0.9}Gd_{0.1}O_{1.95}$ (Ref. 7)		$2.3x10^{-2}$	$1.2x10^{-2}$	$4.5x10^{-3}$
$La_{0.9}Sr_{0.1}Ga_{0.9}Mg_{0.1}O_{2.9}$ (Ref. 7)		$2.5x10^{-2}$	$1.5x10^{-2}$	$4.5x10^{-3}$

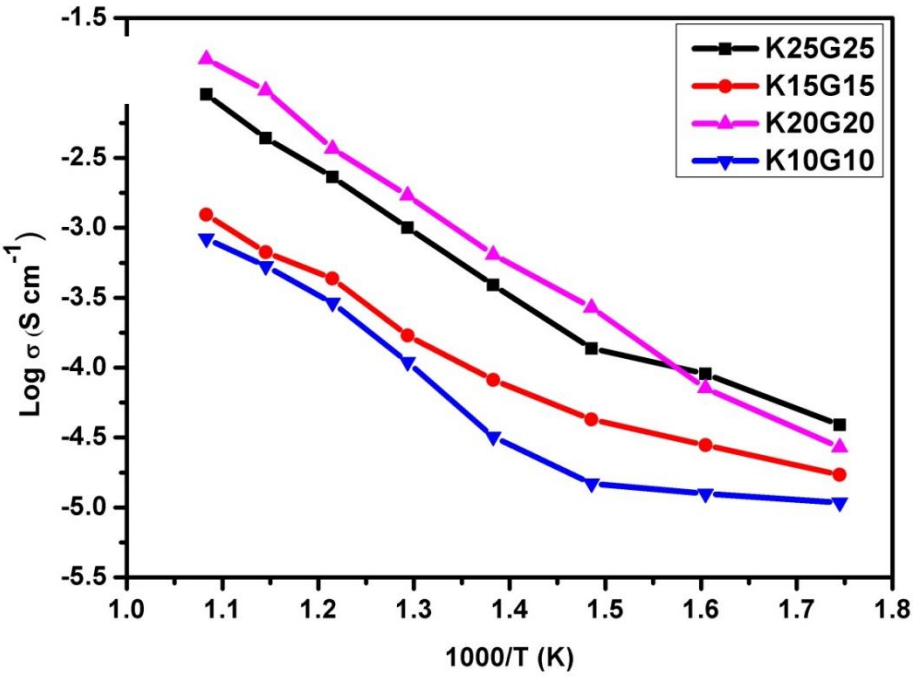

Figure 4.8 Arrhenius plot for different composition of K and Ga substituted $BaZrO_3$ i.e. (i) $Ba_{0.9}K_{0.1}Zr_{0.9}Ga_{0.1}O_{2.9}$ (K10G10) (ii) $Ba_{0.85}K_{0.15}Zr_{0.85}Ga_{0.15}O_{2.85}$ (K15G15) (iii) $Ba_{0.8}K_{0.2}Zr_{0.8}Ga_{0.2}O_{2.8}$(K20G20) (iv) $Ba_{0.75}K_{0.25}Zr_{0.75}Ga_{0.25}O_{2.74.}$(K25G25)

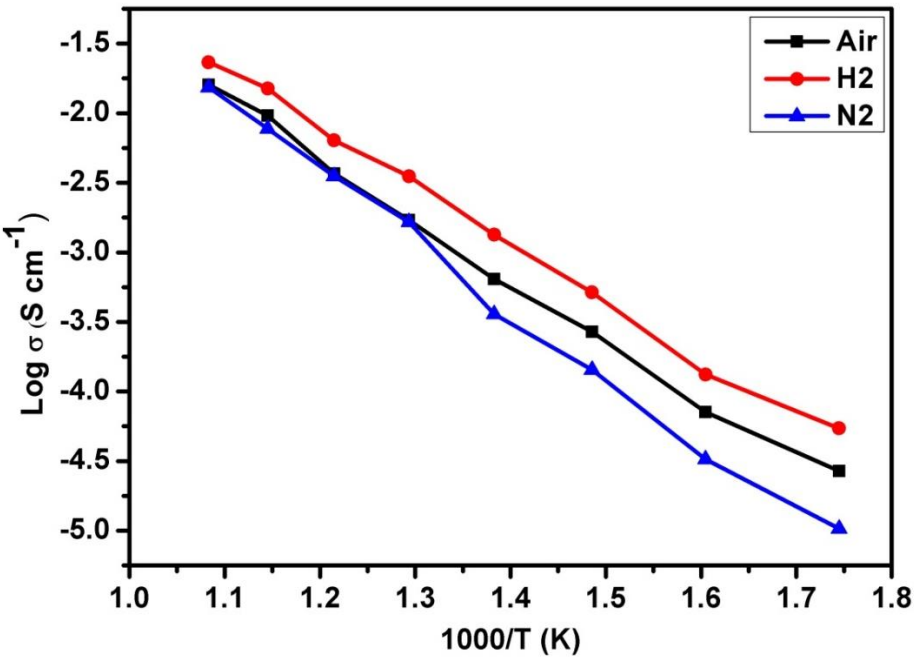

Figure 4.9. Arrhenius plot of $Ba_{0.8}K_{0.2}Zr_{0.8}Ga_{0.2}O_{2.8}$ (BKGZO) in different medium

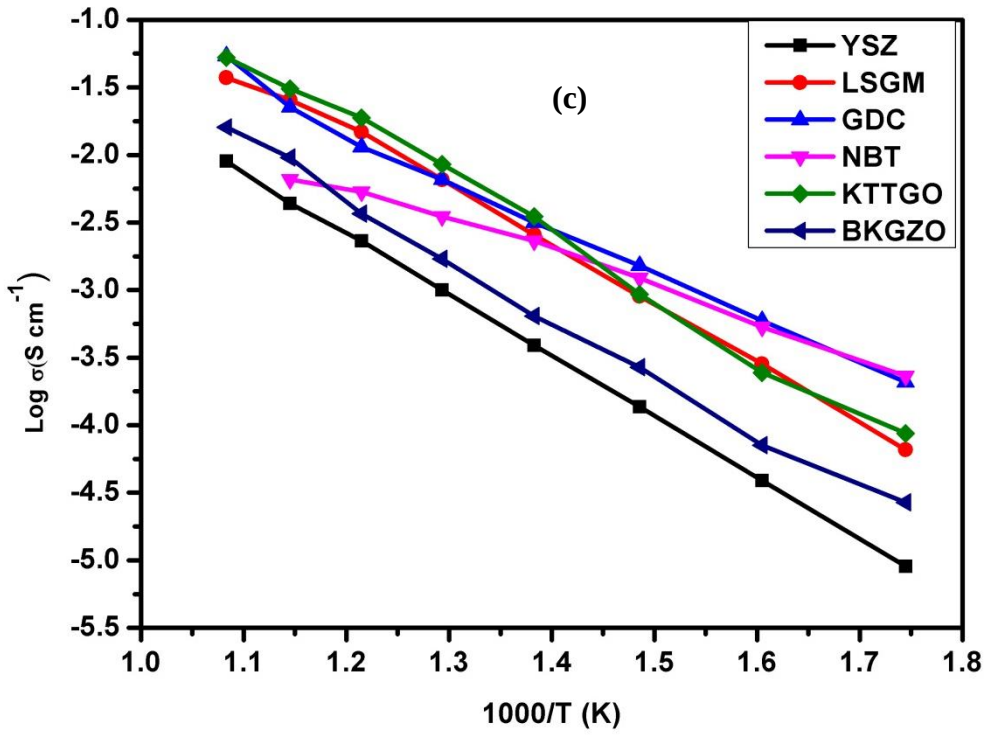

Figure 4.10. comparison of ionic conductivities of existing intermediate temperature Oxide-ion electrolytes in the air from Ref. 7 & 10

Figure 4.8 shows the Arrhenius plots of total electrical conductivity of $Ba_{1-x}K_xZr_{1-y}Ga_yO_{2-\delta}$ perovskite series with varying potassium and gallium concentration. The conductivity values are plotted against the 1000/T factor, and the slope is calculated by linearly fitting the curve using origin pro software. From the obtained slope, the activation energy is calculated using the following equation:

$$\sigma T = \sigma 0 \exp(\frac{-Ea}{kT}) \qquad \text{Eq (4.3)}$$

Where σ_0 is the pre-exponential factor, E_a is the activation energy, k is the Boltzman constant, and T is the absolute temperature. The average thickness of each pellet was 0.25 cm. The variation in total conductivity with respect to dopant concentration at various measured temperatures is depicted in figure 4.8. Except for $Ba_{0.8}K_{0.2}Zr_{0.8}Ga_{0.2}O_{2.8}$ sample, two activation regions were found in K and Ga doped $BaZrO_3$ sample as there is a sharp increase in conductivity of all the samples above 400^{o}C. The activation energy for oxide-ion

conductivity was found to be as low as 0.43 eV for the $Ba_{0.8}K_{0.2}Zr_{0.8}Ga_{0.2}O_{2.8}$ sample. Activation energies for all the samples are provided in table 4.3.

Table 4.3 Activation Energy of $Ba_{1-x}K_xZr_{1-y}Ga_yO_{3-\delta}$

	Activation Energy(eV)	
Compound	***UPTO 400°C***	**ABOVE 400°C**
$Ba_{0.9}K_{0.1}Zr_{0.9}Ga_{0.1}O_{2.9}$	2.24	0.48
$Ba_{0.85}K_{0.15}Zr_{0.85}Ga_{0.15}O_{2.85}$	0.45	0.44
$Ba_{0.8}K_{0.2}Zr_{0.8}Ga_{0.2}O_{2.8}$	**0.43**	**0.43**
$Ba_{0.75}K_{0.25}Zr_{0.75}Ga_{0.25}O_{2.7}$	1.92	0.47

The conductivity of $Ba_{0.8}K_{0.2}Zr_{0.8}Ga_{0.2}O_{2.8}$ was also measured in hydrogen (UHP H_2) and Nitrogen (UHP N_2) environment (Figure 4.9) to see the effect of the absorbed moisture, hydrogen and oxygen on the surface of the sample. Below 500°C, the total conductivity of $Ba_{0.8}K_{0.2}Zr_{0.8}Ga_{0.2}O_{2.8}$ was found to be lower in the Nitrogen atmosphere compared to air. This may be due to the fact that some absorbed moisture or hydroxide-ions present in the sample can contribute to the additional protonic type conductivity at lower temperatures. The higher conductivity above 600°C (the no weight loss region in TGA, Figure 4.5) in a non-humidified environment confirms that the conductivity of the materials at higher temperature is predominantly due to oxide-ion vacancies. Thus it can be concluded that at temperatures (T ≥600°C), the ionic conductivity of the material is mainly due to oxide-ion vacancies. The cole-cole plot at 500°C for $Ba_{0.8}K_{0.2}Zr_{0.8}Ga_{0.2}O_{2.8}$ is shown for understanding the polarization

and to understand the oxide-ion transport nature (Figure 4.11). Almost linear tails of the cole-cole plot at lower frequencies clearly demonstrate ionic contribution in the conductivity.

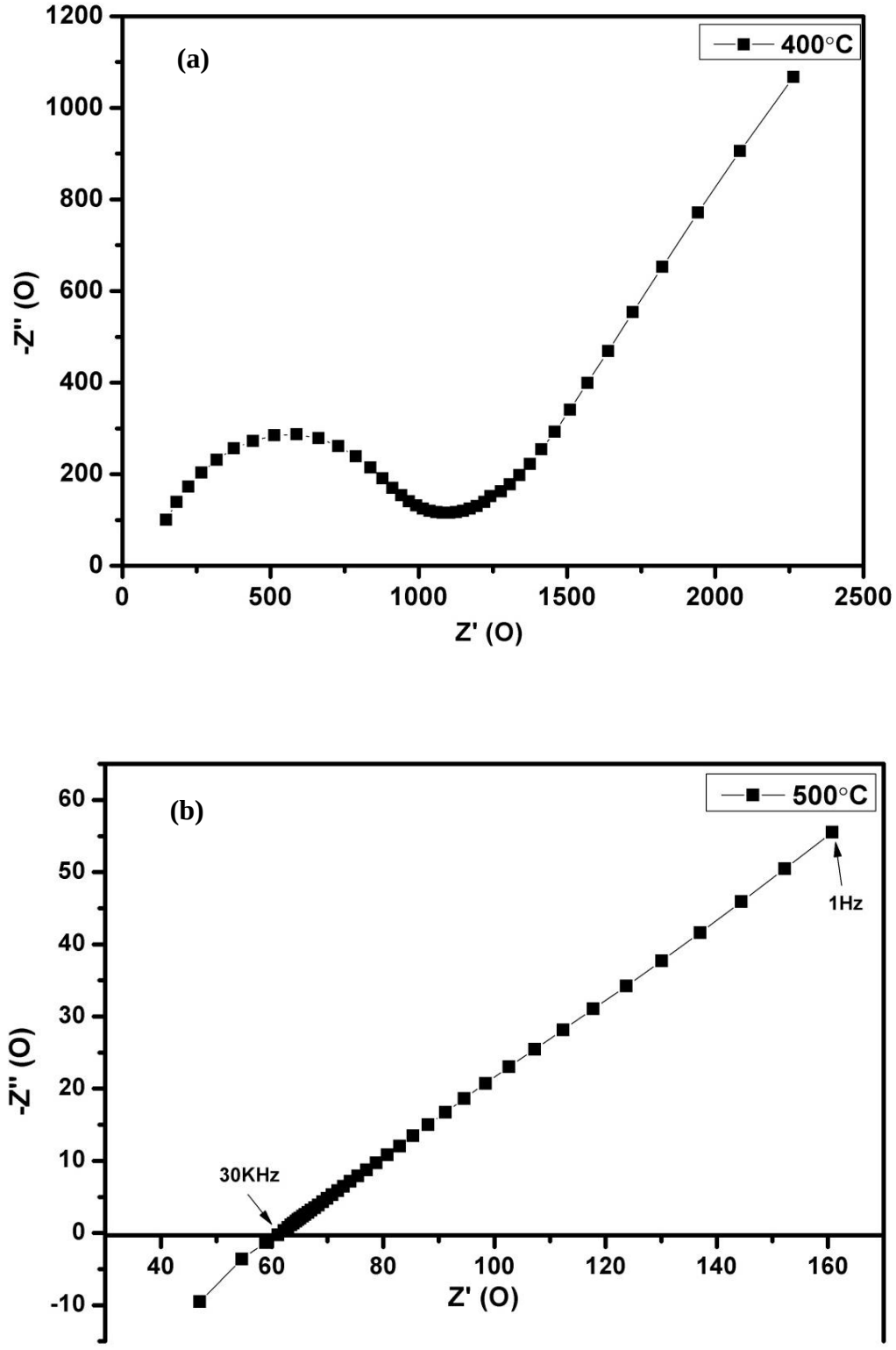

Figure 4.11 Cole-Cole plot of $Ba_{0.8}K_{0.2}Zr_{0.8}Ga_{0.2}O_{2.8}$ at(a) 400 ^{o}C, (b) 500 ^{o}C.

4.4 Conclusion

It can be concluded that substitutions of K and Ga at Ba and Zr Sites, respectively, in $BaZrO_3$ lattice resulted in stoichiometric oxide-ion vacancy type point defect formation. The oxide-ion vacancy formation resulted in superior ionic conductivity above 600^oC in non-humidified atmospheres. It helped the material to overcome the poor ionic conductivity problem at elevated temperatures ($T > 500^oC$), which limits the material's application as a conductive electrolyte for ceramic fuel cells. The oxide-ion conductivities obtained here for simultaneously K and Ga doped $BaZrO_3$ samples are superior or equivalent to the conductivity obtained for YSZ (yttria-stabilized zirconia); a well-known ceramic oxide-ion electrolyte. The material can also be explored in a high moisture-rich or humidified environment for applications as a protonic conductor for ceramic fuel cells and hydrogen separating membrane formations.